Journal of Applied Fluid Mechanics, Vol. 18, No. 11, pp. 2757-2774, 2025.
Available online at www.jafmonline.net, ISSN 1735-3572, EISSN 1735-3645.
https://doi.org/10.47176/jafm.18.11.3456

Coupling Mechanisms Between Vortex Rope Evolution and Cavitation Within the Draft Tube of Pump-turbines

L. Xin[1], Q. Li[1,2†] and S. Zhang[3]

[1] *College of Energy and Power Engineering, Lanzhou University of Technology, Lanzhou, Gansu Province, 730050*
[2] *Key Laboratory of Fluid Machinery and Systems, Lanzhou, Gansu, 730050, China*
[3] *Tianjin Tianfa Heavy Hydropower Equipment Manufacturing Co., LTD, Tianjin, 300400, China*

†*Corresponding Author Email: lqfy@lut.edu.cn*

ABSTRACT

A technique integrating numerical simulations with experimental observations was hereby employed to elucidate the flow instability mechanisms during transient processes in pump-turbines, and a reversible pump-turbine was investigated for in-depth insights. Concurrently, the coupling phenomena between vortex rope and cavitation under transient conditions were systematically analysed. The results indicate that rotational and pressure gradients predominantly drive the vortex rope evolution, thereby exerting a substantial influence on cavitation development. The formation and collapse of low-pressure cavities disrupt the vortex structures while intensifying the flow instability. High tangential momentum as well as shear layers contribute to forming alternating vortex structures. Cavitation bubbles are either entrained by the vortex rope or diffuse outward, resulting in pronounced fluctuations in cavity volume. As the vortex structure evolves, it gradually transitions downstream into a more stable, axisymmetric configuration. Pressure fluctuation analysis reveals that low-frequency oscillations within the straight conical section are predominantly induced by vortex rope rotation and cavitation collapse. In the elbow region, localized pressure amplification arises from vortex-wall interactions, while the axial non-uniformity of vortex ropes and cavity distribution governs the spatial variability of pressure pulsations. Collectively, this study establishes a theoretical basis for understanding the coupling between vortex ropes and cavitation. It further offers practical guidance for controlling vortex dynamics and mitigating cavitation in engineering applications.

Article History

Received February 24, 2025
Revised April 28, 2025
Accepted June 21, 2025
Available online September 3, 2025

Keywords:

Pump-turbine
Draft tube
Cavitation vortex rope
Transient flow
Pressure pulsation

1. Introduction

As global energy transition evolves, particularly in the context of China's "dual carbon" goals and expansion of renewable energy, pumped-storage power technology is emerging as a cornerstone of modern power systems. These facilities hold considerable significance in mitigating the variability inherent in renewable energy generation. In grid operations, pumped-storage power stations serve critical roles such as peak shaving, valley filling, and emergency standby, while also representing one of the most effective solutions for large-scale energy storage. The increasing development regarding intermittent renewable energy sources in recent years has significantly heightened the grid's requirements for real-time power balancing and dynamic regulation. Leveraging its superior stability and flexibility, pumped-storage technology has become indispensable for mitigating renewable energy fluctuations and maintaining grid stability. To satisfy grid regulation requirements, pumped-storage units undergo frequent start-stop cycles and alternate between power generation and pumping modes This operational pattern amplifies stability challenges during unit operation. Under low-load conditions or when operating outside the non-vortex zone, vortex rope phenomena are more likely to occur. These vortex ropes disrupt flow the field characteristics and trigger intense pressure pulsations, causing adverse effects on hydroturbine components and markedly diminishing both operational stability and economic performance. In extreme scenarios, excessive pressure pulsations can cause equipment damage and plant vibrations, posing substantial risks to power station safety (Kavurmaci et al., 2017; Qi, 2017).

The formation, development, influencing factors, and instability of vortex bands in tailpipes have been

extensively studied by research scholars. In particular, during the 1950s, Leingans carried out the first - ever model experiments on hydraulic turbines and methodically examined the dynamic behaviours of the vortex line within the draft tube when the turbine operated at reduced load. The outcomes showed that the frequency of pressure pulsations in the drawworks was roughly 1/3.6 of the turbine's rotational speed (Li, 2025). Favey & Cassidy (1970) delved into the impact of cavitation on pressure pulsations using experimental methods. Liu (2024) discovered in model tests that in instances involving a low cavitation number of the model, distinct vortex rope shapes appeared in tailpipes. Tacob & Liu (1998) analysed five typical running commands of a pump turbine, mainly through experiments, and summarised the involution of the vortex bands in the tailpipe as the running controls change. Their research uncovered the presence of noticeable vortex ropes in the partial load condition, with nonlinear changes in pressure pulsation amplitudes. Chen et al. (2006) employed PIV to measure the internal flow within the draft pipe. They observed the emergence of a ring - shaped flow pattern near the centre of the conical section, oriented perpendicular to the measurement plane. The intensity of the ring-shaped flow increased as the guide vane opening decreased, and a noticeable backflow region was noticed in this area. Liu et al. (2006) delved into the pressure changes in the tailpipe's straight conical section of a pump turbine during a transient process and analysed the reasons for the development of vortex bands. Fanelli (1989) observed vortex bands in tailpipes through tests and determined the association between the bent elbow's structure and the vortex bands' shape. Qu & Wang (1996) conducted model tests on varying operating conditions of mixed-flow pump-turbines under medium and low head, analysing the pulsation characteristics in draft-tube. Liu et al. (2016) explored the pressure pulsation characteristics in the tailwater pipe under rotor braking via unit tests and determined the change rule of pressure amplitude and band of frequency at the monitoring point when the guide vane opening varied. He et al. (2002) collected pressure data in the pump-turbine tailpipe under diverse service regimes and systematically verified the relationship between the magnitude of pressure fluctuations and operating conditions. Tiwari et al. (2020) discovered through model tests that the amplitude of fluctuations within the draft tube reached its peak when the unit operated at 0.55 times the optimal flow rate. Later, Wei (1997) experimentally established a relationship between the magnitude of pressure fluctuations in the tailwater pipe and the position of the vortex core.

Over the years, experimental research has been recognised as the primary method for analysing pressure waves within the draft tube (Chen, 2017; Zhou, 2024). However, the experimental method is costly and arduous, and is constrained by environmental factors and modelling accuracy. With rapid advances in fluid mechanics software, researchers have integrated experimental and numerical modelling to facilitate a more comprehensive comprehension of the pressure characteristics induced by vortex ropes in draft tubes. Specifically, Susan et al. (2006) employed the LDV (Laser Doppler Velocimetry) technique in a model test to measure the streamline distribution within the tailrace of a Francis turbine under 17 operating scenarios. The accuracy of numerical simulations was validated using different vortex models. While this method confirmed the simulation accuracy with experimental data, additional analysis of the internal flow patterns inside the draft pipe remained required. Han et al. (2006) applied the RSM method for simulating the retractor tube and successfully predicted the distribution of vortex cords and dead zones. Liao et al. (2008) examined the relationship between vortex ropes and pressure across different guide vane settings. Their work demonstrated how turbine operating conditions impact the pressure pulsation patterns within the draft tube. Concurrently, existing research have explored the application of simplified models. For instance, Luo et al. (2008) conducted steady-state numerical simulations to study the vortex ropes within the draft tube of an turbine without including the runner. However, the simulation results were limited as they did not account for the runner's influence. Huang et al. (2011) utilized CFD to investigate the water hammer and cavitation phenomena within the turbine. They employed the cavitation gas fraction to depict the characteristics of the vortex ropes and conducted an analysis of the relationship between the Thomas coefficient and vortex ropes. To improve simulation accuracy, researchers have started to use a variety of turbulence models. Specifically, Qian & Huang (2006) delved into the impacts of alternative turbulence models on the characteristics of an eddy line in a towpath tube. Li et al. (2010) incorporated simulations into experimental studies. They discovered that that as the runner speed increased, both the volume and intensity of the vortex in towpath tube increased. Yang (2011) investigated the air-cavitation number affecting the whirling ropes and revealed the reasons for the formation of whirling ropes and their effects through the results of the gas-phase distribution. Mulu et al. (2012) investigated the location of maximum axial velocity change under different loading conditions using Doppler speedometer in model tests. Zuo et al. (2014) employed the RNG k-ε fluid dynamics model along with the air erosion model to forecast the pressure fluctuations induced by the rotating vortex filament in the draft tubes of Francis turbines. The results showed that the system was in the absolute instability region under part-load regimes. Guo et al. (2007) utilized the LES for the simulation of computational domains both with and without the draft tube. They successfully predicted the cavitation phenomena in the outflow pipe. Dragica & Lipej (2011) compared the prediction accuracy of pressure amplitudes under different guide vane openings using the RSM, SST, and LES models. Tamura et al. (2014) combined experimental studies to investigate the interplay between the passage outlet and transient cavitation vortex ropes in the draft pipe. Alekseenko (2016) and Skripkin et al. (2016, 2017) compared the conversion process between varying vortex structures in elbow and conical draft tubes. They analysed the frequency relationships, conversion processes, and variations in pressure pulsation amplitude for both single and double vortex ropes. This was achieved through pressure measurements and laser beam measurements of the rotation frequencies of the vortex

ropes. They observed the phenomenon of reconnection when single vortex ropes form vortex rings, which led to strong pressure pulsations. Goyal et al. (2017a,b) investigated the formation of vortex ridges in the drawworks during load shedding in a high-head Francis turbine using the PIV technique. They discovered that the hysteresis zone at the centre of the drawworks, along with the relatively high gradient of the velocity in the vertical direction, played a role in the formation of the vortex rope. Litvinov et al. (2018) explored the instability of vortex structures using vortex generator rapid prototyping and computer measurement techniques in conjunction with laser dweller tachometry to analyse the change in velocity distribution inside the drafting tube under non-design terms. Collectively, these studies highlight the importance of numerical simulations in vortex rope research and emphasise the indispensable role of multiphase flow and turbulence models in simulating vortex ropes, providing theoretical and methodological support for further exploration of complex flow patterns in the draft tube.

While current studies on pump-turbine draft tubes have independently investigated vortex ropes and cavitation phenomena, the dynamic coupling characteristics between these two have not been adequately explored. Cavitation phenomena, which manifest during the formation and evolution of vortex ropes, are capable of triggering intricate variations in pressure pulsations and vibration characteristics through significant feedback from the flow field. However, the specific mechanisms underlying this coupling effect and its influence on system stability remain poorly understood. Moreover, while existing studies have established that low-frequency pressure pulsations induced by vortex ropes significantly impact equipment operational stability, in-depth and detailed studies regarding the variation patterns and underlying mechanisms of pressure pulsations under the interaction between vortex ropes and cavitation are still lacking.

To address these issues, this study combines experimental observations and numerical simulations for a pump-turbine unit. The investigation systematically studies the effect of interactions between vortex ropes and cavitation in drawtubes and their influence on pressure pulsation variations. The transient characteristics of the coupling effect between vortex and cavitation under complex flow conditions are elucidated, facilitating the understanding of internal flow mechanisms in pump-turbines. These findings forge a theoretical foundation for advancing the study of unsteady flow patterns in draft tubes, optimizing pump-turbine operating conditions, and supporting the formulation of improved strategies for controlling flow stability.

2. METHODS

2.1 Simulation Framework and Computational Grid

The subject of this study is a mixed-flow pump-turbine. The rated head of the unit at this power station is approximately 200 meters, with a normal water storage level of around 11 meters and an effective storage capacity of approximately 1300 cubic meters. Both the upstream and downstream are equipped with surge chambers. In order to carry out three-dimensional transient process analysis, a computational domain model was hereby developed. This model includes key constructions such as vortex channel, fixed and movable guide vane, flow channel and draft tube. The construction of the unit is shown in Fig. 1, and Table 1 presents the values of the values of the modelled construction.

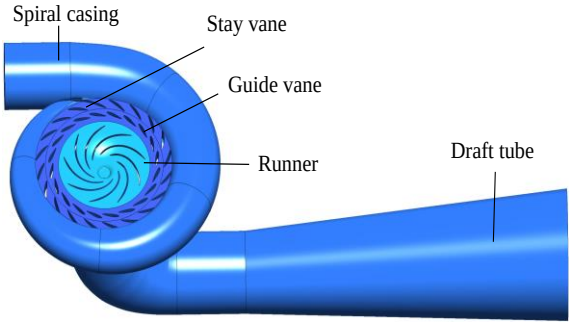

Fig. 1 Pump-turbine computational domain

Table 1 Pump turbine machine basic data

Variable name	Icon	Numeric size
Runner's diameter on the high-pressure side /mm	D_1	474
Runner's diameter on the low-pressure side /mm	D_2	300
Runner blade count	Z_r	9
Count of guide vanes	Z_g	20
Count of stay vanes	Z_s	20
Draft tube exit diameter /mm	D_{1m}	660
Volute entry diameter /mm	D_{2m}	315
Vane elevation /mm	b_0	66.72
Shell wrap angle/(°)	φ_0	343

To guarantee the accuracy of the calculations, a structured hexahedral mesh was hereby employed to discretize the entire hydraulic model domain. The first level of the grid in the nearside area was set at a height of 0.3 mm. This meshing approach meets the basic requirements for high-precision numerical calculations. Meanwhile, it also provides an accurate boundary layer resolution for subsequent flow analysis, playing a crucial role in turbulence modelling. Figure 2 illustrates the overall mesh layout, while Fig. 3 shows the profile of the dimensional free wall pitch parameter y+ in the near-wall zone.

To guarantee the credibility of the simulations in the S-characteristic situation, a mesh-independence analysis was herby performed, taking half of the rated load as a precondition. Figure 4 illustrates the external characteristics of the unit for various mesh numbers. The performance curve reaches a stable state when the total nodes of the mesh exceed 6.5 million. Based on the preceding analyses and with the objective of achieving the most favourable equilibrium between computational precision and efficiency, after thorough consideration, a mesh containing approximately 6.6 million nodes was

Table 2 Details of grid division

Region	Spiral Casing & Stay vane	Guide vane	Runner	Draft tube
Grid number	1921768	1357611	1612376	1675129
Total nodes	409253	1129135	1232182	1592017
Min angle /(°)	19	30	27	36
Minimum mass	0.49	0.49	0.53	0.65

Table 3 Comparison of simulation and test results: n_{t11} represents the unit speed in the experimental test (r/min), Q_{t11} denotes the unit flow in the experimental test (m^3/s), n_{s11} represents the unit speed in the simulation (r/min), and Q_{s11} denotes the unit flow in the simulation (m^3/s)

Condition	Turbulence model	n_{t11}	Q_{t11}	n_{s11}	Q_{s11}	Δn_{11}	ΔQ_{11}
OP. 1	SST *k-ω*	47.133	0.771	45.641	0.755	3.16	1.95
	Standard *k-ω*	47.133	0.771	45.430	0.751	3.61	2.47
	Realizable *k-ε*	47.133	0.771	45.733	0.753	2.97	2.21
OP. 2	SST *k-ω*	72.256	0.520	70.292	0.504	2.71	3.04
	Standard *k-ω*	72.256	0.520	69.894	0.501	3.27	3.66
	Realizable *k-ε*	72.256	0.520	70.281	0.504	2.73	3.08

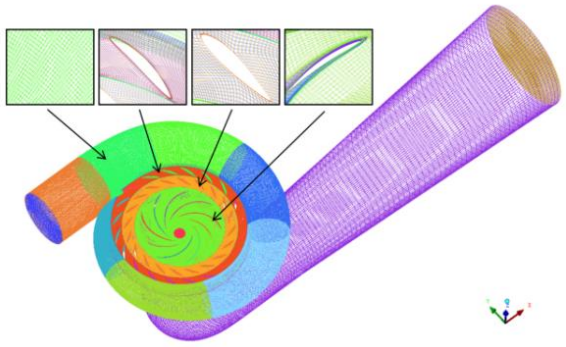

Fig. 2 Illustration of the local grid

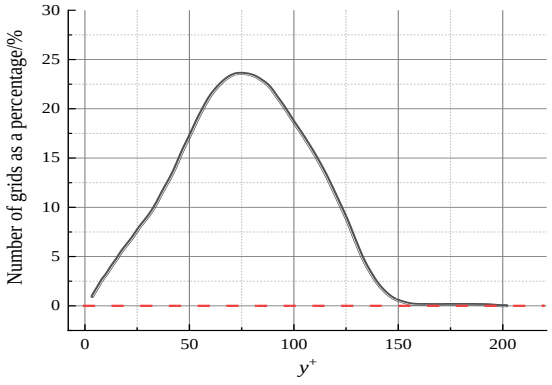

Fig. 3 Plot of near-wall y+ value distribution

chosen for the subsequent simulations. The specific parameters of this mesh are provided in Table 2.

2.2 Turbulence Model Selection

Under un-engineered conditions, the airflow inside the draft tube is predominantly affected by the vortex structure. Hence, the selection of an appropriate turbulence model is of paramount importance for accurately simulating the flow field. This is particularly

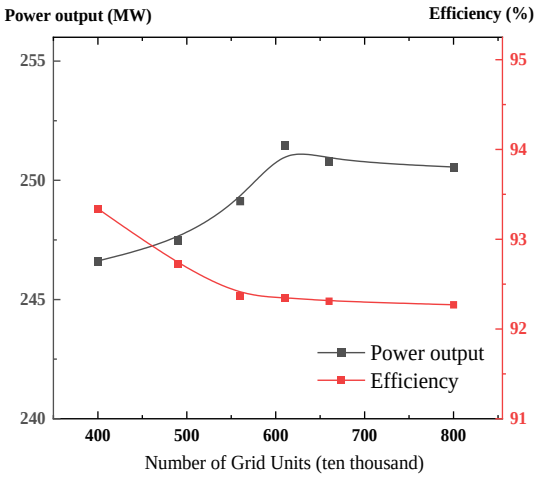

Fig. 4 Verification of grid independence

critical when investigating the coupling effects of vortex ropes and cavitation in pump-turbines.

Simulations were hereby conducted using different turbulence models, and the results are summarized in Table 3. Compared to conventional turbulence models, the SST *k-ω* model demonstrates significant advantages, yielding the smallest relative error with respect to experimental data. This model effectively combines the near-wall accuracy of the *k-ω* model with the numerical stability of the *k-ε* model in free shear flows. As such, it more accurately captures complex flow features such as vortex separation, boundary layer shear stress, and local backflow induced by cavitation. These characteristics make the SST *k-ω* model particularly suitable for simulating unsteady internal flows in pump-turbines.

In pump-turbine studies, numerical simulation results generally exhibit a slight excess over the experimental values. The primary cause of this divergence is attributed to the idealization of simulation conditions. Numerical simulations often neglect factors such as sealing leakage, surface roughness, and local flow separation,

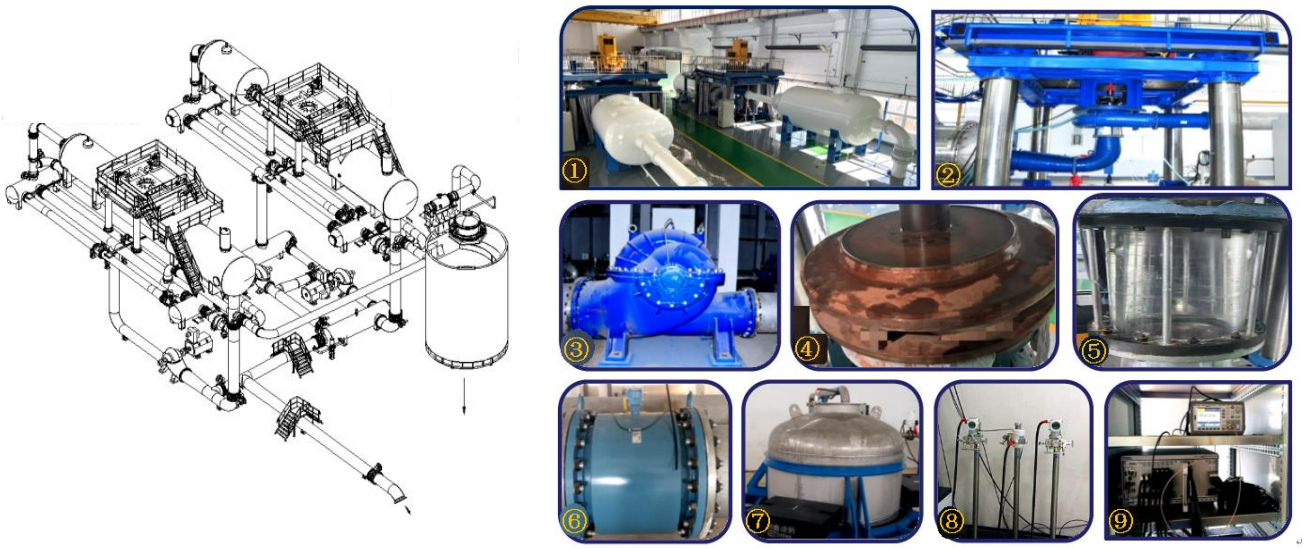

Fig. 5 Schematic diagram of reversible hydraulic turbine laboratory stage: (1) Laboratory Hall, (2) Main Pump-Turbine, (3) Main Power Pump, (4) Test Runner Structure, (5) Visualization Section of the Straight Conical Segment, (6) Meter, (7) Flow Calibration Weigh Barrel, (8) Measurement Gauge Head, and (9) Data Acquisition Box

which lead to energy losses in actual operation, thereby resulting in overestimated flow rates or efficiency. Additionally, turbulence models are subjected to certain limitations in predicting resistance losses, which may further underestimate actual energy dissipation. These factors collectively account for the deviation between the numerical simulation results and experimental values.

The entry boundaries conditions were assigned by the mass flow volumes, while the exit was defined as a free-flow outflow. During the structured meshing process, immovable boundary conditions were imposed on the walls. The data transfer between computational domains was handled via a matched-pair interface. The frame of reference pressure was maintained as standard atmospheric pressure, and a default loosening factor was utilized. In the solution process, the SIMPLEC algorithm was employed in conjunction with a second-order upwind scheme. An unsteady time step of $\Delta t = 3.932\times10^{-4}$ s was adopted, and iterative calculations were conducted with a convergence criterion of 10^{-6}.

For the numerical simulation of cavitation, most existing approaches are building upon the homogeneous mixture theory, which assumes that the liquid and vapor stages are uniformly mixed with different densities, while neglecting the relative motion between the two phases. The Zwart model, sourced from a simplified form of the Rayleigh-Plesset bubble dynamics equation, defines the mass transfer rate through the following equation:

$$m=\begin{cases} F_e \dfrac{3\alpha_{nuc}(1-\alpha_v)\rho_v}{R_s}\sqrt{\dfrac{2}{3}\dfrac{p_v-p}{\rho_l}} & (p \le p_v) \\ F_c \dfrac{3\alpha_v\rho_v}{R_B}\sqrt{\dfrac{2}{3}\dfrac{p-p_v}{\rho_l}} & (p > p_v) \end{cases} \tag{1}$$

where P_v denotes the vapor pressure, ρ_v is the vapor density, and α_{nuc} represents the volume fraction of vapor nuclei, R_B refers to the theoretical radius of the nuclei, and F_e and F_c are empirical correction coefficients for vaporization and condensation, respectively, with typical values of 50 and 0.01. As the vapor volume fraction increases, the number density of nuclei per unit volume decreases, introducing a mathematical asymmetry between vaporization and condensation. To address this, the condensation term incorporates the vapor volume fraction α_v, whereas the vaporization term is adjusted using the expression $\alpha_{nuc}(1-\alpha_v)$. This modification more accurately reflects the distinct behaviours of vapor nuclei during two-phase transitions.

2.3 Experimental Correlation

Figure 5 presents the pump-turbine test rig used in this project, which was furnished by the Tianjin Key Laboratory for Hydropower Machinery. Designed for hydraulic machinery models, the platform integrates the TFGT and TTFDT systems, both operating as closed-loop systems with the flexibility to function in open or closed modes. It is equipped with precision sensors for measuring flow, pressure, absolute pressure and moment, facilitating in-situ calibration. This setup supports comprehensive performance testing and allows for bidirectional flow meter calibration.

The primary components of the unit are fabricated from metal. The transparent acrylic tailwater cone facilitates direct inspection of the flow pattern at the outlet of the runner and inside the cone of header water. The dimensional deviation of the model is kept within the permissible limits specified in the IEC norms. Table 4 summarises the test parameters to ensure optimum

Table 4 Parameters of the experimental platform

Main pump type	34S4-19×1
Highest head / m	30
Maximum flow / (m^3/s)	2.0
Rotor diameter / (mm)	380
Generator power / (kW)	540
Engine RPM / (r/min)	0–2600
Main pump motor power / (kW)	593
Driving pump speed / (r/min)	0–1200
Volume of flow calibration vessel / (m^3)	120 × 2
Storage capacity / (m^3)	750

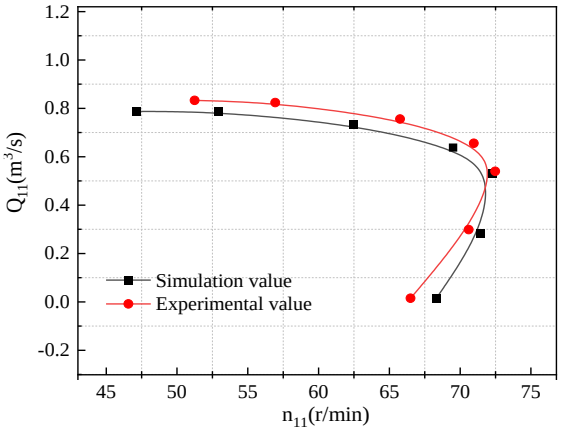

Fig. 6 Experiment versus modelled 'S' characteristic zones

utilisation of the platform and reliable experimental results.

In this study, to validate the computational model and method for the S-curve region, several key operating points were selected from the comprehensive characteristic curve for detailed analysis. Employing experimental data and simulation parameters, the unit speed (n), as well as inlet mass flow rate (q_m) were hereby computed following Equations (2) and (3). The computed findings were then compared with the experimental measurements.

$$n_{11} = \frac{nD_2}{\sqrt{H}} \tag{2}$$

$$Q_{11} = \frac{Q}{D_2^2\sqrt{H}} \tag{3}$$

where H stands for the test head (m), D_2 represents the impeller diameter (m)'s low-pressure side, Q represents the flow rate (m^3/s), while n refers to the rotational speed (r/min). Additionally, n_{11} and Q_{11} refers to the rotational speed of the unit. (r/min) as well as unit discharge (m^3/s), respectively.

As shown in Fig. 6, the n_{11}-Q_{11} curves of the analogue and laboratory data uncover a high degree of agreement. The values closely match the experimental measurement results, mainly attributed to instrumental

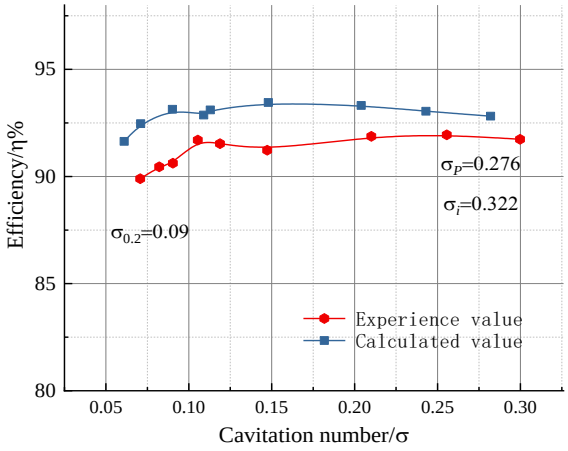

Fig. 7 Cavitation performance curve comparison

limitations and minor deviations caused by procedural factors. The largest relative error is kept within 2.7%, further confirming the accuracy of the computational method, the methodology, and the test setup.

The procedures were executed in accordance with the GB/T 3216-2005 standard. During the experiment, the flow rate was maintained at a constant level, and the tailwater pipe's inlet pressure was incrementally reduced to enhance the vacuum degree at the inlet, thereby triggering cavitation within the unit. With a further decline in the inlet pressure, cavitation intensified, particularly in the cavitation zone on the blade surface, resulting in a substantial reduction in pump efficiency. The cavitation number (σ) was introduced as a variable to characterize the cavitation phenomenon, facilitating data processing and calculations.

$$\sigma = \frac{P_{in} - P_v}{0.5\rho u_2^2} \tag{4}$$

In the given formula, P_{in} denotes the inlet pressure (Pa), P_v corresponds to the vapor pressure at equilibrium (Pa), and ρ is the density of the working fluid (kg/m^3). Additionally, u_2 represents the tangential velocity at the impeller outlet (m/s).

As illustrated in Fig. 7, the numerical calculations and experimental results exhibit similar trends, with discrepancies remaining within an acceptable range. This demonstrates the numerical model's reliability in predicting the pump-turbine's cavitation performance under varying cavitation number conditions. The discrepancy between experimental and simulated cavitation performance curves primarily arises from model simplifications, insufficient mesh resolution in critical flow regions, the neglect of thermal coupling effects, and measurement uncertainties. In numerical simulations, conventional cavitation models often overlook thermodynamic effects such as heat absorption during vapor formation and temperature changes during bubble collapse. This absence of thermal coupling can lead to local pressure prediction errors, especially under severe or near-critical cavitation conditions. On the experimental side, variations in sensor accuracy and fluid

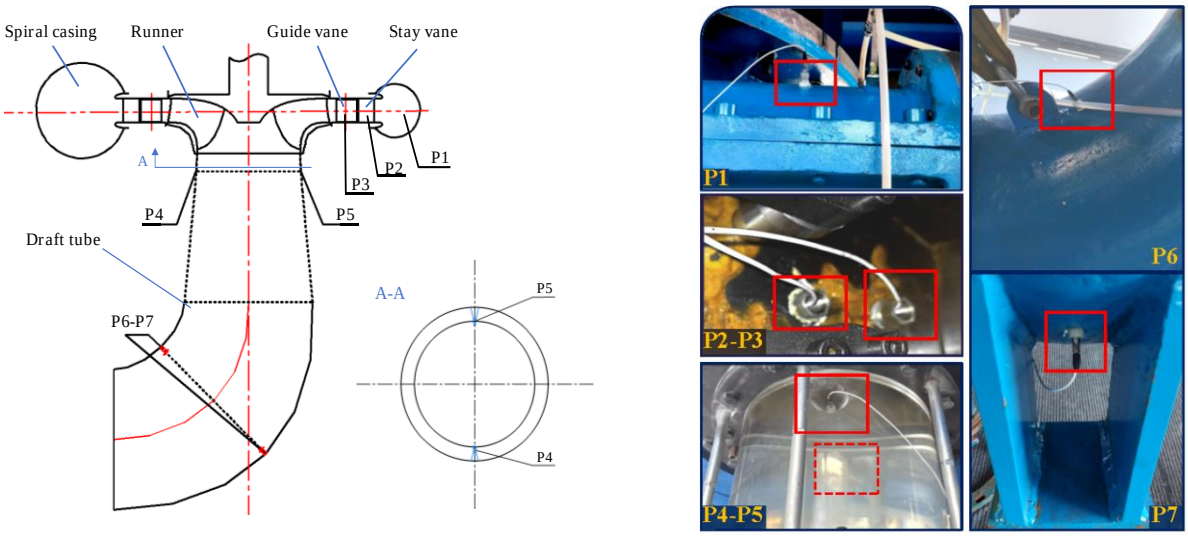

Fig. 8 Arrangement of pressure pulsation monitoring locations in the pump-turbine model includes: (1) the volute inlet; (2) the runner region adjacent to the upper cover and within the blade-passing zone; (3) the straight conical section of the draft tube; (4) the elbow area of the draft tube

Table 5 Pressure pulsation measurements during model turbine operational testing

Location of monitoring sites	Working condition	Results ($\Delta H \cdot H^{-1}$)	Warranty value ($\Delta H \cdot H^{-1}$)
Between movable, fixed guide vanes	Rated working condition Operation Under Partial Load Conditions	0.84 2	＜3% ＜3%
Leafless area		4.82 4.205	＜7% ＜6%
leaf top clearance	Rated working condition Operation at Partial or No Load Conditions	1.77 2.69	＜7% ＜7%
Draft tube	Runs under ideal conditions Partial duty	0.55 1.035	＜2% ＜6%

properties may also contribute to deviations in the cavitation curve.

2.4 Pressure Pulsation Analysis

Pressure oscillations within the flow field serve as a crucial diagnostic parameter for assessing the operational integrity and dynamic behavior of hydraulic machinery. These oscillations, particularly under transient conditions, can be significantly intensified by the evolution and interaction of cavitating vortex ropes in the draft tube. Such phenomena introduce complex unsteady loads and pose risks to structural stability and system reliability. Therefore, obtaining accurate and high-resolution pulsation data—both from numerical simulations and physical experiments-is essential for understanding flow instabilities and guiding optimization. In the experimental configuration, pressure sensors were strategically deployed at key hydraulic passages, including the inlet of the spiral casing, the guide vane region, the runner passage, and the draft tube elbow (as shown in Fig. 8). These monitoring points were selected based on their sensitivity comprehensive analysis of pressure wave propagation and its coupling with vortex structures throughout the entire to pressure fluctuations and cavitation activity, enabling a flow domain.

To ensure the reliability of the pressure fluctuation analysis, numerical simulations were systematically validated against experimental observations, with comprehensive results summarized in Tables 5 and 6. Critical monitoring locations included the inlet of the spiral casing, the transition zone from guide vanes to runner channels, the region above the primary flow path, and the draft tube section. All measurements were conducted in accordance with the standards specified in GB/T 15613 (2008) and IEC 60193, under multiple representative operating conditions. The numerical framework exhibited high predictive accuracy, and in conjunction with empirical data, the total measurement uncertainty of the TFGT model test apparatus was determined to be 0.16%, well within the allowable engineering tolerance.

3. Calculation And Analysis Results

3.1 Cavitation Vortex Rope Evolution Study

The vortex rope represents a macroscopic flow phenomenon and serves as a comprehensive manifestation of the vorticity field within the draft tube. Figure 9 depicts

Table 6 Experimental value of draft tube pressure pulsation

Monitoring position	f (Hz)	f_n (Hz)	$\Delta H \cdot H^{-1}$ (%)	$f \cdot f_n^{-1}$
Prior to the Draft Tube Cone	3.14	18	1.92	0.2
Beyond the Draft Tube Cone	3.14	18	1.87	0.2
Upstream side of the elbow pipe	299.86	18	0.4	17
Downstream side of the elbow pipe	162.05	18	0.83	9

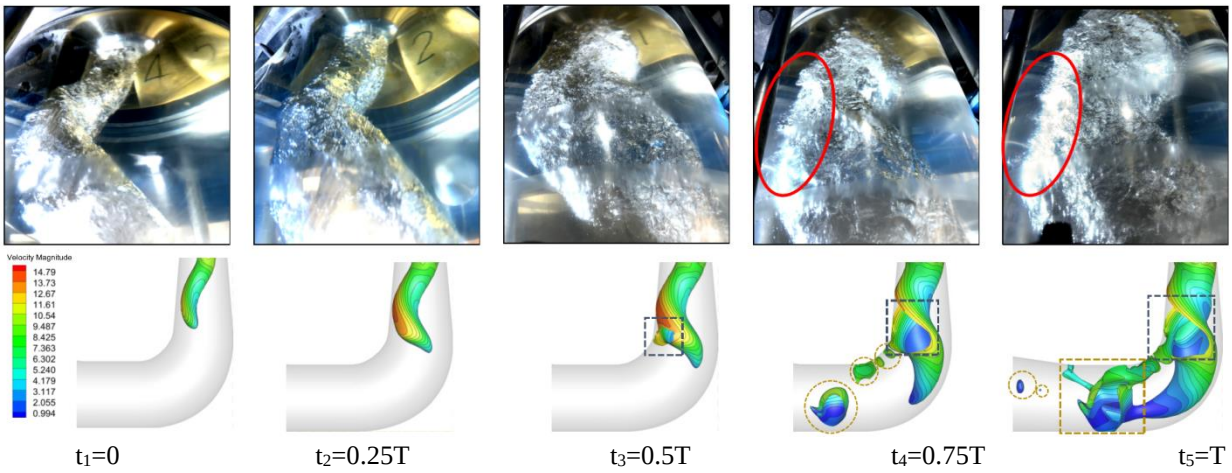

Fig. 9 Vortex string morphology in draft tube

the vortex rope's evolution over a single cycle within the draft tube. At the initial stage (t_1), the vortex filament forms within the straight conical section, primarily driven by the rotational flow generated at the pump-turbine runner outlet and influenced by the draft tube geometry. At this stage, the vortex rope exhibits smooth boundaries as well as a uniform velocity distribution. Simultaneously, a strong rotational core appears within the vortex, resembling the classical Rankine vortex structure and characterized by high vorticity intensity and pronounced rotational rates. This flow phase remains relatively stable, primarily governed by the draft tube geometry and incoming flow velocity.

As the vortex rope evolves (t_2), its boundaries undergo significant stretching and curling. These morphological changes are primarily influenced by the Coriolis effect and velocity gradients. As the fluid traverses downstream along the curved draft tube wall, the nonuniform velocity distribution induces transverse velocity gradients, promoting vortex stretching. Simultaneously, the curling phenomenon reflects substantial shear stress near the vortex filament, contributing to the elongation and oscillation of the vortex along the flow direction. The stretching and twisting of the vortex rope are additionally affected by local pressure fluctuations. These fluctuations stem from instabilities induced by changes in guide vane openings and velocity disparities at fluid interfaces.

During the t_3-t_4 phase, the vortex rope begins to disintegrate due to the impact of the draft tube structure. This disintegration gives rise to the formation of low-pressure zones. When the pressure becomes lower than the vapor pressure of the liquid, localized cavitation develops, forming vapor bubbles that move along with the vortex rope. Low pressure zones in the vortex bundle result directly from rotational effects, inducing abrupt velocity variations within the core. Centrifugal forces generate substantial velocity gradients in the vicinity of the vortex bundle, which further decreases the pressure at its central region. This phenomenon conforms to Bernoulli's principle in fluid dynamics. The unstable positioning of low-pressure zones within the vortex rope causes temporal variations in the occurrence and expansion of cavitation bubbles.

During the later evolutionary stage (t_5), significant tearing and reconstruction of the vortex rope take place in regions with abrupt pressure changes. This phenomenon arises from the formation and collapse of cavitation bubbles within the vortex rope, generating transient local pressure spikes that destabilize the vortex structure. The collapse of cavitation bubbles generates shock waves that impinge upon the vortex rope boundaries, causing it to break up into smaller vortex structures. A portion of these smaller vortices dissipates into localised turbulent flows. Shock waves from bubble collapse induce intense transient pressure fluctuations in the surrounding fluid. Meanwhile, bubble collapse amplifies the flow instability of the swirled rope, leading to its unravelling and reorganisation.

Figure 10 presents a conceptual schematic designed to enhance understanding of the formation mechanism of cavitating vortex ropes within the draft tube. The evolution process is typically divided into three distinct stages: initiation, growth, and collapse. In the early phase (Fig. 10-a), a localized pressure reduction—often induced by flow separation or adverse pressure gradients-leads to cavitation inception. At this stage, vapor bubbles begin to form and interact with the emerging helical vortex

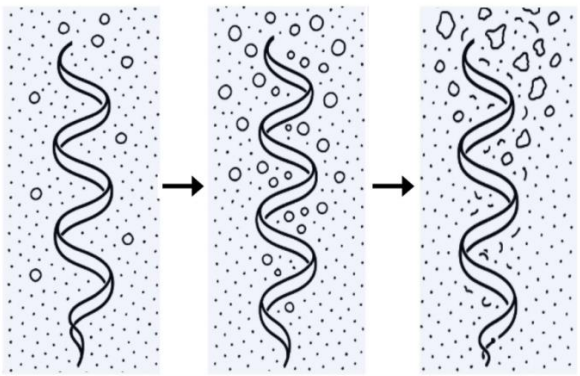

(a) Formation (b) Development (c) Collapse

Fig. 10 Schematic diagram of nascent development and collapse of cavitation vortex belt

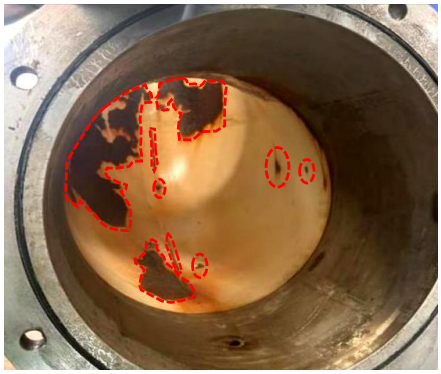

Fig. 11 Damage to the bend section of the draft pipe

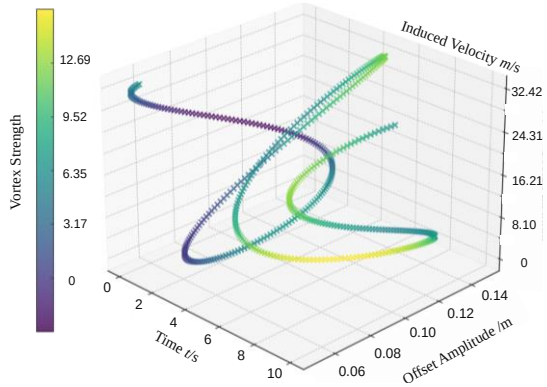

Fig. 12 Dynamic interaction of vortex parameters over time

structure. These bubbles tend to co-rotate with the swirling flow, exhibiting pronounced fluid-structure interaction characteristics and amplifying local flow instabilities.

As the flow continues to destabilize, the cavitation region enlarges progressively, driven by both centrifugal effects and persistent low-pressure zones within the vortex core. This results in the development of a coherent, well-organized cavitating vortex rope, as shown in Fig. 10-b. The structure becomes increasingly energetic and pronounced, often dominating the draft tube flow field and contributing to enhanced pressure pulsations.

Eventually, in the collapse stage (Fig. 10-c), sudden pressure recovery-either due to downstream pressure fluctuations or vortex breakdown—forces the vapor bubbles to implode. This collapse process is often violent, releasing stored vapor-phase energy and generating strong localized pressure shocks. Such dynamic behavior not only contributes to flow-induced vibrations but may also induce structural excitation and potential resonance effects. The entire sequence highlights the highly coupled, nonlinear dynamics between cavitation phenomena and vortex evolution, which are critical in understanding draft tube instability mechanisms.

The coupling between cavitation and swirling ropes generates periodic pressure flux on the wall of the draft pipe elbow, which affects the flow stability and the structural safety of the system. As illustrated in Fig. 11, the complex interactions between unsteady flow structures-such as vortex ropes and cavitation bubbles-and the surrounding fluid can induce significant pressure fluctuations and high-frequency impacts on the inner surface of the draft tube, particularly in the elbow region.

Over time, these dynamic loads may result in localized wall erosion, material fatigue, or even structural damage, highlighting the critical importance of accurately capturing and analyzing these phenomena during both design and operation stages.

Figure 12 illustrates the relationships among vortex rope offset amplitude, induced velocity, time, and vorticity strength, with the latter visualized through a colour map.

This comprehensive depiction, derived from experimental and numerical simulation data, captures the dynamic behaviour of the vortex bundle region. The variations in the vortex rope's offset amplitude highlight complex coupling effects within the flow field. Notably, substantial offset amplitudes are indicative of flow instability in the draft tube. When the local flow field is influenced by the vortex's induced velocity, the low-pressure zone undergoes a discernible positional shift, leading to pronounced variations in the offset amplitude. At approximately 3.5 and 6 seconds, the vortex rope's offset amplitude peaks within the conical section of draft tube. This behaviour is predominantly driven by the wake circulation from the blades and the geometric constraints of the draft pipe. Conversely, when the offset amplitude diminishes, the vortex core has a tendency to return to a symmetric alignment. This realignment enables the pressure inside the draft pipe to become more stable. Dynamic changes in offset amplitude result in uneven velocity distribution around the vortex, which leads to an asymmetric spatial distribution of cavitation bubbles in the low-pressure zone. This asymmetry impacts both the intensity of cavitation and its spatial localization. Additionally, increased offset amplitude exacerbates interactions between the vortex rope and cavitation bubbles, intensifying flow instability within the draft tube. These fluctuations in offset amplitude can also induce pressure pulsations and thus pose potential risks to system stability.

The induced velocity of the vortex rope emerges as a key parameter for evaluating its influence on the surrounding flow field. Fluctuations in induced velocity reflect the intensity of disturbances within the shear layer and directly indicate the vortex's dynamic impact. Elevated induced velocities amplify localized cavitation phenomena, evidenced by their temporal fluctuations, as shown in Fig. 11. These fluctuations demonstrate the dynamic interplay between the rotational core and the fluid boundary. The intensity of such interactions is governed by variations in the offset amplitude of the vortex rope. Due to fluid inertia effects, changes in induced velocity lag behind offset amplitude fluctuations, as observed in the 0.07-0.11 m range. Vorticity strength represents the rotational intensity of the vortex core. It exhibits periodic oscillations closely correlated with offset amplitude. Peak vorticity strength is observed when offset amplitude and induced velocity are at their maxima. However, as the vortex rope approaches the draft tube wall, vorticity strength diminishes due to the viscous effects of the surrounding fluid. This further results in asymmetric oscillations. Stronger vortices generate pronounced low-pressure zones, which are key contributors to cavitation. When vorticity exceeds a critical threshold, cavitation bubble generation accelerates; conversely, reduced vorticity can lead to bubble collapse. The interplay between induced velocity and cavitation is notable. Higher induced velocities exacerbate cavitation, whereas cavitation increases disturbances in the shear layer, thereby augmenting induced velocities. These interactions, coupled with variations in vorticity strength, determine the location and intensity of cavitation. They can also initiate pressure pulsations within the draft tube, compromising system stability. By analysing time-scale curves, the coupling mechanisms between vortex ropes and cavitation are quantitatively elucidated. These insights offer a theoretical basis for understanding unsteady draft tube flows and optimizing pump-turbine performance.

3.2 Analysis of Flow Cross-Sectional Diagrams in the Draft Pipe

The analysis of the internal flow field is essential not only because it directly reveals the flow characteristics within the pump-turbine system, but also because it provides an indispensable approach for understanding the underlying mechanisms responsible for the formation and evolution of macroscopic flow phenomena such as vortex ropes, cavitation, and flow separation. These phenomena significantly affect the hydraulic performance and operational stability of the unit. By closely examining the internal flow field, one can gain insights into how these complex fluid behaviors emerge, interact, and evolve under varying operational conditions. Understanding the spatial and temporal dynamics of the flow is crucial for identifying regions of high turbulence, pressure fluctuations, and flow instabilities, which may lead to potential issues like vibrations or efficiency losses. Figure 13 presents a thorough investigation of the internal flow field by extracting key cross-sections from the draft tube, where critical flow behaviors, such as the interaction between vortex ropes and cavitation, are particularly evident. These cross-sectional views allow for a detailed

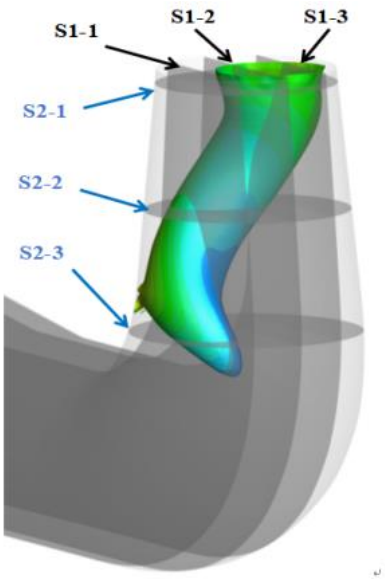

Fig. 13 Section of the drawing tube

visualization of the flow structure and provide a foundation for identifying the root causes of performance degradation, offering valuable data for future design improvements and operational optimizations.

Figure 14 presents the pressure distribution within draft tube, highlighting significant variations in the vortex region. At the S1 cross-section, a distinct low-pressure zone (blue to green areas) forms in the vortex rope core due to centrifugal forces. The pressure values range from approximately -30,645 Pa (dark blue) to -480.774 Pa (light green). As the vortex rope extends downstream, the pressure transitions into positive values (yellow to red), peaking at approximately 39,738.3 Pa. In three circular cross-sections along the Z-axis (S2 interfaces), the pressure contours at various downstream positions illustrate the pressure evolution within the vortex core. At the S2-1 cross-section, the vortex rope core appears as a pronounced low-pressure ring structure, characterized by concentrated and intense negative pressures. As the vortex rope evolves morphologically, the S2-2 cross-section exhibits a reduction in radial velocity, accompanied by a partial recovery in pressure. While the low-pressure ring weakens, it persists visibly. The pressure gradually shifts from negative to positive values, accompanied by a concurrent decrease in vortex intensity. At the S2-3 cross-section, which is located within the straight-conical and elbow segments, the ring-shaped pressure structure dissipates, leading to a more homogeneous overall pressure distribution.

In the vortex rope flow field, a marked increase in local dynamic pressure is typically coupled with a significant drop in static pressure, creating the pronounced low pressure zone in the core. According to the vorticity equation in fluid mechanics, this phenomenon results from intense tangential rotational motion, where tangential velocity considerably exceeds axial velocity. This imbalance causes a rapid decline in local static pressure, forming a steep pressure gradient characteristic of turbulent vortex ropes. The periodic variation of the

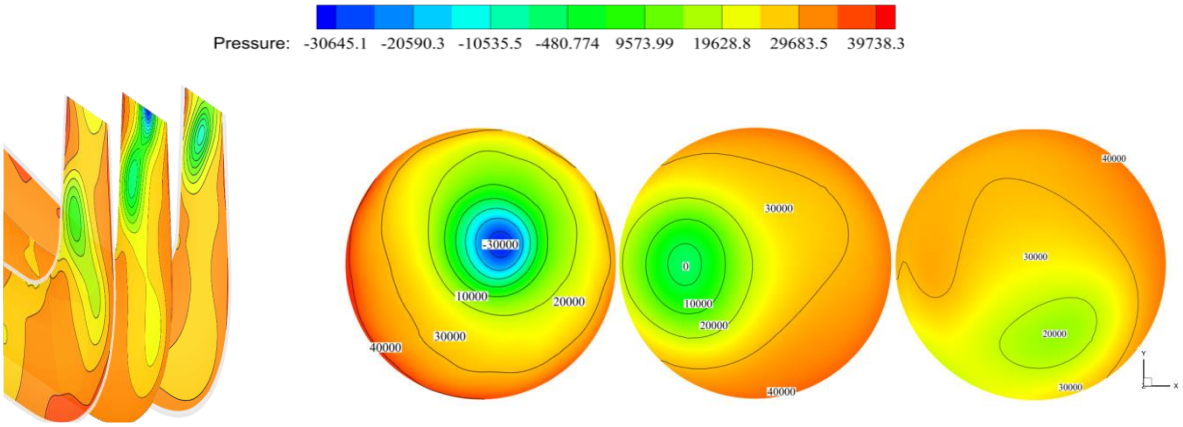

(a) Sections S1-1, S1-2, and S1-3 (b) Sections S2-1, S2-2, and S2-3

Fig. 14 Pressure contour plots at different sections of the draft tube

vortex filament induces cyclic fluctuations in draft pipe pressure distribution, strongly associated with cavitation formation and evolution. The low-pressure regions, particularly within the vortex core, drop beneath liquid's vapor pressure, thereby establishing conditions favourable for cavitation. Under such conditions, water undergoes rapid phase transition, generating cavitation bubbles. As the vortex rope oscillates periodically, these bubbles form and collapse within the core region, releasing pressure fluctuations. As a result, these fluctuations interact with the surrounding flow field, significantly impacting the intensity and dynamic characteristics of the cavitation process within the draft tube.

The non-uniform pressure distribution exacerbates flow instability and intensifies cavitation effects. The formation of cavitation generates bubbles and modifies local fluid characteristics (e.g., density and viscosity). These variations affect the vortex rope's structure and evolution, reinforcing the coupling between vortices and cavitation. This complex interaction amplifies flow instability, leading to heightened pressure oscillations, potential structural vibrations, and reduced system stability and efficiency. The interplay between the vortex rope and cavitation not only increases flow complexity but also amplifies pressure fluctuations. This leads to elevated vibrations and a decline in the pump-turbine system's hydraulic performance.

The high-speed rotating vortices are intimately linked to the growth and instability of vortex ropes in the draft tube. Analysing the vorticity evolution is essential for better elucidating the internal flow structures and the dynamic characteristics of vortex bundle distribution. Figure 15 presents the vorticity contour plots for various sections within the draft tube, where colour indicates the rotational direction of vortices, and black lines represent the vortex line directions. Vorticity serves as the microscopic foundation of the vortex rope, with its distribution reflecting the flow's non-uniformity and complexity. The alternating red and blue regions in the vorticity plots denote strong rotational flow structures, including counter-rotating vortices, and significant changes in vortex line directions. The intricate and shifting vortex structures mainly arise from the interaction between the shear flow exiting the runner and the walls of the draft tube. Non-axisymmetric flow at the blade outlet, combined with the secondary flow carrying high angular momentum under off-design conditions, is the primary cause of the complex vorticity distribution observed in this region. The high-energy, high-rotation-speed flow at the blade outlet generates a pronounced shear layer at the draft tube entrance, thereby inducing Kelvin-Helmholtz instability. This further evolves into refined vortex structures. Moreover, the boundary layer near the draft tube wall, especially in the upstream portion of the conical section, generates localized counter-rotating vortices, adding further complexity to the overall vorticity distribution.

Downstream, the S2-2 cross-section exhibits a gradual reduction in vorticity complexity. The red regions, representing counter-rotating vortices, noticeably converge toward the central region. Concurrently, the blue regions, indicative of vortices with a single rotational direction, dominate. The high-momentum fluid from the runner outlet gradually propagates into the draft tube, suppressing local counter-rotating vortices. According to the Vorticity Transport Equation, the momentum convection term becomes dominant at this location, leading to the annihilation of counter-rotating vortices by the primary vortices. At the S2-3 cross-section, the vorticity plot is predominantly characterized by vortices with a single rotational direction (blue regions), signalling the increasing stabilization and symmetry of the field. The axial symmetry of the flow improves, with asymmetry diminishing substantially and counter-rotating vortices almost disappearing. According to the Vorticity Transport Equation, the turbulent dissipation term starts to exert a more dominant influence, weakening the strength of the remaining vortices. Furthermore, the energy released by cavitation collapse excites high-wavenumber turbulence components in the vorticity field, causing rapid decay of vortex energy. The low-pressure regions associated with cavitation suppress the formation of new counter-rotating vortices and enhance vorticity dissipation through gas-

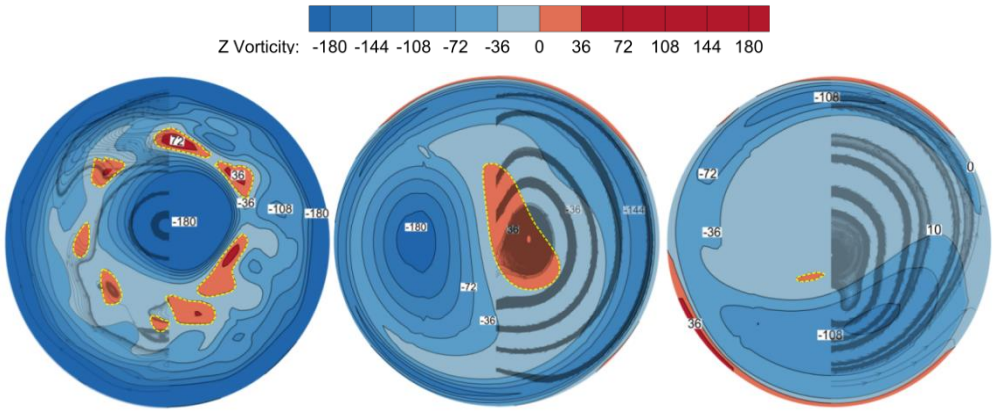

(a) Sections S2-1, S2-2, and S2-3

(b) Vortex line trajectory details

Fig. 15 Vorticity contour map at cross-sections of the draft tube

liquid interfacial friction. This further results in the gradual loss of vortex rope complexity in the downstream region. As counter-rotating vortices weaken and dissipate, the vortex flows within the draft tube become more regular. This development of symmetry reflects the dynamic transition of the flow from instability to stability. The periodic variations in vorticity drive oscillations in the vortex rope, which, in turn, affect pressure fluctuations and flow field distribution within the draft tube. Vorticity offers a microscopic viewpoint for studying rotational flow characteristics, whereas the vortex rope embodies the macroscopic accumulation of vorticity. These two aspects are inherently interconnected in the dynamic study of the draft tube flow field.

3.3 Variation of Cavitation Bubble Volume Under the Vortex Core Evolution

Analyzing the temporal variation of vapor volume fraction is essential for understanding the dynamic evolution of cavitating vortex ropes and their impact on pump-turbine performance. Cavitation is inherently unsteady, influenced by factors such as fluid dynamics, pressure fluctuations, and system vibrations. Tracking the temporal changes in vapor volume fraction reveals the formation, expansion, and collapse of cavitating vortex ropes under various conditions. This provides crucial data for studying the interaction between cavitation, the flow field, and vibrations. By examining these time-dependent variations, we can identify transient cavitation characteristics, which support system optimization and fault diagnosis, ultimately enhancing pump-turbine efficiency and reliability.

As shown in the vapour volume fraction cloud in Fig. 16, the periodic rotation of the vortex cords can result in an uneven local pressure split at the inlet of the vent pipe. Regions characterized by higher vorticity are capable of giving rise to localized reductions in pressure. These pressure decreases, in turn, trigger cavitation formation. The low-pressure areas within the vortex rope core correspond closely with those of high vapor volume fraction. This suggests that the vortex rope intensifies local cavitation. The vapor distribution at the draft tube inlet is non-uniform due to the entrainment and distribution effects of the helical vortex structure. The configuration and behavior of the vortex rope have a direct impact on the cavitation distribution within the flow field. The stretching and rotational motion of the vortex rope can transport vapor from high-cavitation regions to areas with lower cavitation, contributing to the observed distribution irregularities. A "cavitation capture zone" may form in the core and surrounding areas of the vortex rope, where vapor is either entrained or diffused outward. As a result, local vapor volume variations are further influenced. Additionally, the shear layer between the outlet and the draft pipe inlet exacerbates the uneven cavitation distribution. Fluctuations in vorticity within the shear layer cause vapor to either aggregate or disperse.

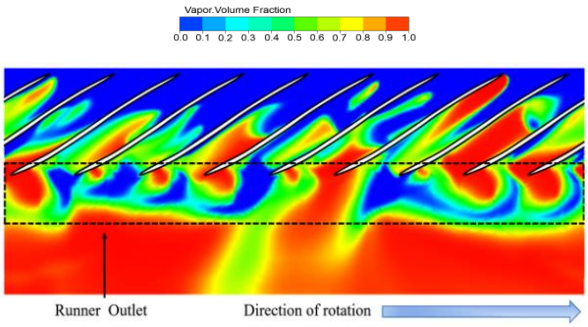

Fig. 16. Cavitation bubble volume contour map

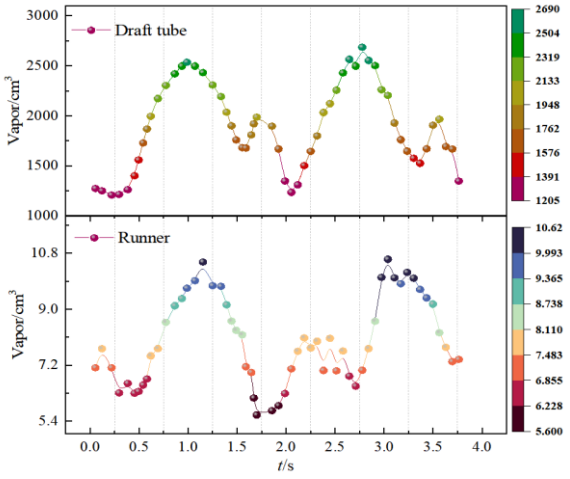

Fig. 17 Variation of cavitation bubble volume in the runner and the draft pipe region

When vapor clusters in the shear layer, it leads to an increase in cavitation intensity.

Figure 17 illustrates the variation of cavitation volume (in cm³) withwithin the draft tube and runner regions at varying time points (t/s). The figure presents time-series data that capture the fluctuations in cavitation volume over time, highlighting how pressure changes associated with the evolution of the helical vortex structure influence cavitation behaviour in the flow field. Within the draft tube region, the cavitation volume exhibits pronounced oscillatory behaviour. As shown, volumes peak at approximately 1.1 s and 2.7 s, reaching around 2,690 cm³ and 2,504 cm³, respectively. These peaks suggest that significant pressure fluctuations take place within the draft tube at those moments, triggering marked cavitation development. Throughout the entire 0.0-4.0 s interval, the cavitation volume within the draft tube displays a periodic rise-and-fall pattern, increasing from a minimum of 1,205 cm³ to peak values. This pattern clearly reflects the periodic influence of vortex rope rotation and localized pressure variations on cavitation generation and evolution. Such cyclical behaviour indicates a strong correlation between cavitation dynamics and large-scale vortex structures within the draft tube. Particularly, during phases where the vortex rope intensifies and local pressure drops rapidly, cavitation bubbles tend to expand dramatically. Conversely, when the vortex weakens or shifts position, the bubbles collapse swiftly, causing sharp changes in volume over short timescales. This suggests that the frequency and amplitude of cavitation volume fluctuations are predominantly controlled by the dynamic behavior of the vortex rope in the draft tube, including its rotational speed, suction strength, and spatial movement.

In contrast, the variation of cavitation volume in the runner region shows a relatively steady pattern. The maximum volume reaches approximately 10.3 cm³ (around 1.1 s), while the minimum is roughly 5.6 cm³. This suggests that despite the presence of cavitation in this region, the overall extent of its fluctuations is rather restricted. Cavitation in the runner region is primarily influenced by the downstream vortex rope, especially through secondary vortices or local flow disturbances it induces, which results in mild cavitation activity. However, its contribution to the overall flow disturbance and energy loss is significantly lower compared to that of the draft tube region. A quantitative comparison reveals that the amplitude of cavitation volume fluctuations within the draft tube is approximately 280 times greater than that in the runner. This finding further validates that cavitation within the draft tube is significantly more intense and acts as the main contributor to energy dissipation and unsteady excitation within the system. This phenomenon is particularly prominent in the diffuser section, where large-scale helical vortices form robustly and exhibit unstable behaviour. As a result, this area is more susceptible to generating cavitation events with large volumes and high frequencies.

The cavitation volume in the flow passage region exhibits more distinct frequency variations compared to the draft tube. This is primarily due to the high rotational speed in the passage, which intensifies shear and tensile effects on cavitation structures. Additionally, the complex flow near the blade trailing edges, characterized by local backflow and vortex shedding, amplifies the instantaneous fluctuations of cavitation volume. This coupling may excite cavitation at specific frequency components. From a phase perspective, the flow passage region lags behind the draft tube. This lag arises because the dynamic changes in cavitation volume within the penstock feedback through pressure waves that influence the outlet pressure of the passage. Owing to fluid inertia, pressure waves propagating from the draft tube to the passage region experience a delay, resulting in an observable phase difference. In the draft tube, the evolution of the vortex rope primarily drives cavitation generation and development, while the corresponding pressure field response in the passage follows subsequently. This leads to the observed lag in cavitation volume variation. Such a phase lag reflects the complex dynamic interaction between vortex rope–cavitation coupling and pressure field feedback. It also underscores the decisive role of vortex rope formation, displacement, and dissipation in shaping cavitation behaviour within the draft tube. The structural evolution of the vortex not only governs the periodic fluctuations of local pressure but also directly triggers oscillations in cavitation volume. This, in turn, intensifies both the strength and unsteady nature of cavitation in the draft tube. Such a mechanism reveals a bidirectional coupling relationship between vortex dynamics and cavitation behaviour. These findings lay a theoretical foundation for subsequent research on the unsteady flow within draft tubes, specifically from the viewpoint of fluid-structure interaction. Additionally, it furnishes crucial understanding regarding the cavitation-driven vibration mechanisms and their impact on the stability of hydraulic systems.

3.4 Study of Pressure Pulsations

The pressure pulsation characteristics of large hydraulic units constitutes one of the important indexes to characterize their hydraulic properties. This feature also reflects the complexity of the drainage basin inside

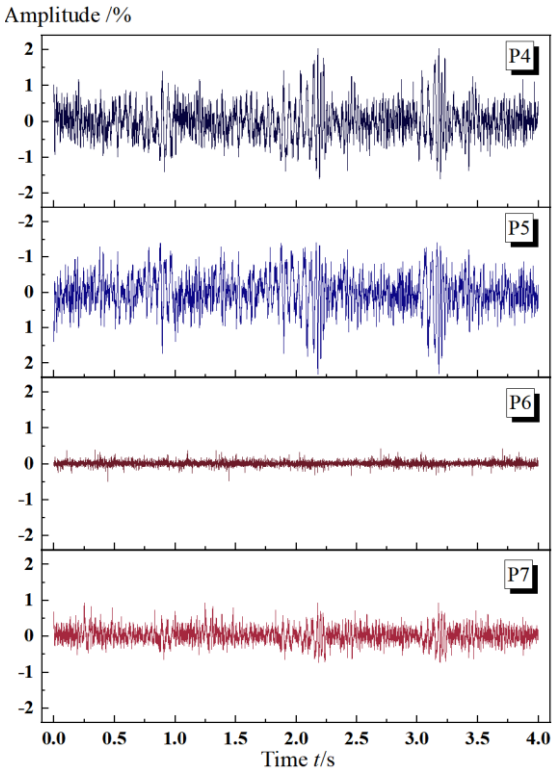

Fig. 18 Time-based pressure fluctuations at monitoring locations

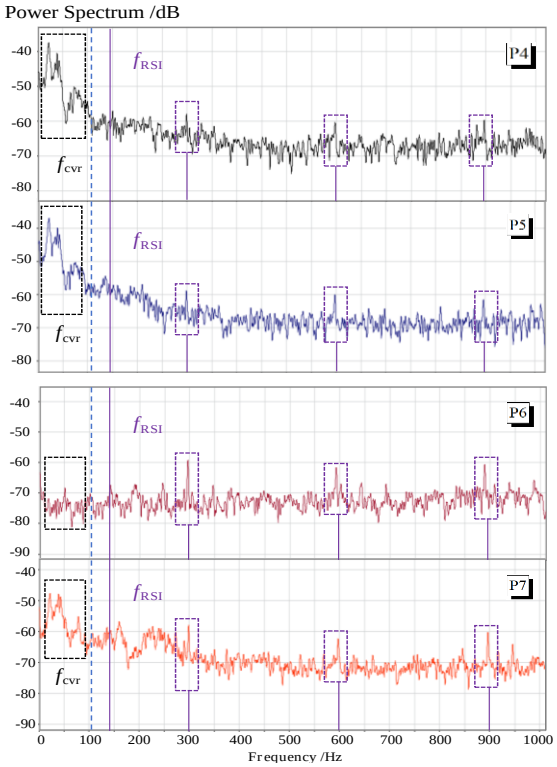

Fig. 19 Frequency-domain pressure fluctuations at monitoring locations

the pump turbine. The non-stationary fluctuations observed in the time-domain graph (Fig. 18) suggest that the pressure field in the draft pipe experiences substantial periodic disturbances. The shear effect of the high-speed rotating fluid, coupled with the cycle of forming and crumbling of air pockets, leads to large localised pressure ripples. Notably, the vibration amplitude is much higher in the straight conical section compared to that in the elbow section. The pronounced fluctuations observed at P4 and P5 highlight the strong coupling between the dynamics of the spiral flow pattern and cavitation. The inlet of the straight conical section, located near the runner outlet, represents the initial region through which the high-speed rotating fluid makes its entry into the draft tube. This region experiences the highest fluid kinetic energy and disturbances, making the between the vortex rope and cavitation with the pressure field particularly impactful. Consequently, vibration vibration levels rise substantially, reflecting the pressure intensity. At stations P6 and P7, the fluctuation characteristics are influenced by the trajectory of vortex rope and geometric constraints. The relatively minor pressure fluctuations observed at P6 imply that this position is less directly affected by the primary vortex rope. It is clear that the pressure fluctuations induced by cavitation weaken with increasing distance from the core of the helical vortex structure.

Figure 19 shows the frequency spectrum of pressure pulsations, with the dominant peak corresponding to the revolution frequency of the vortex rope. Analysis of the internal flow field shows that the flow's asymmetry at the runner outlet, marked by uneven velocity and pressure distributions, leads to high-frequency pulsations in localized areas. A distinct cavitating vortex rope is observed in draft pipe. When this vortex is compressed to the point of sudden collapse, it causes a significant increase in impact pressure. The cavitating vortex rope's dissipation coincides with the absence of high-frequency pulsation signals. This suggests that the source of medium- to bass frequency, high-amplitude pressure pulsations (f_{CVR}) below 6.5 times the runner frequency (f_n) is cavitating flow structure in the draft tube. The runner blade passing frequency and its harmonics (f_{RSI}) continue to impact the pulsation frequencies at the survey points within the draft pipe. Periodic disturbances, such as vortex rope rotation and cavitation collapse, manifest as integer multiple frequency peaks in the spectrum (e.g., 300 Hz, 600 Hz, 900 Hz). The rotation of the vortex and the periodic interference from the guide vanes also produce similar harmonic effects. Moreover, nonlinear dynamic effects within the system, such as turbulence, cavitation, and shear flow, transfer energy from the primary frequency signal (fundamental frequency) to higher frequencies through complex interactions. As a result of these interactions, harmonic signals are produced. When the structural natural frequency closely matches these harmonic frequencies, resonance may occur, amplifying the frequency peaks. This phenomenon highlights the generation and amplification of harmonic signals as direct manifestations of the coupling between complex flow dynamics and structural behaviour in pump-turbines. Specifically, rotational frequency signals are transferred to harmonics through nonlinear effects, with modal resonance within the draft tube further enhancing these harmonic signals. This conclusion not only deepens the comprehension of internal flow mechanisms in pump-turbines but also offers novel perspectives and technical approaches for operation monitoring and fault diagnosis.

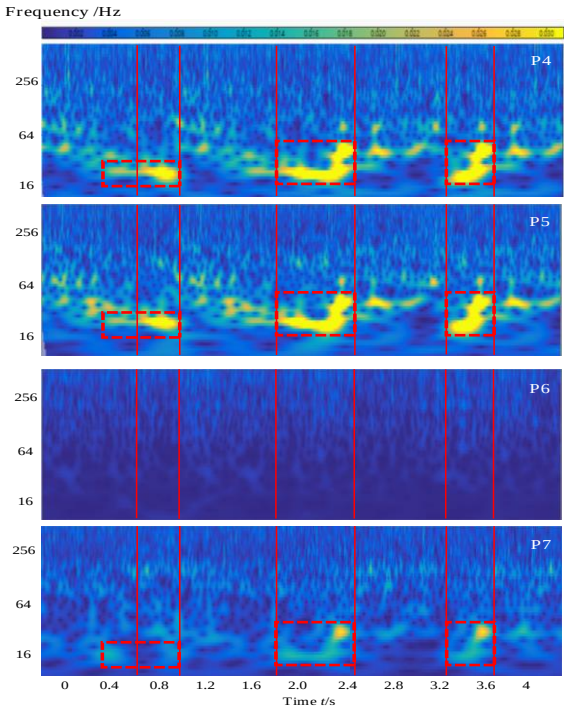

Fig. 20 Time-frequency chart of pressure pulsation monitoring points

Figure 20 displays the time frequency diagrams of pressure pulsations recorded at the monitoring area (P4, P5, P6, and P7), providing a detailed representation of the dynamic pressure fluctuations over both time and frequency domains. These diagrams are crucial for understanding the temporal and spectral behavior of the pressure pulsations within the pump-turbine system. As depicted in the figure, the pressure pulsations exhibit clear periodic oscillations, with the dominant low-frequency characteristics of the cavitating vortex rope being the primary contributor to the sustained spectral energy. In the spectra for monitoring points P4 and P5, distinct bright yellow regions are observed, indicating significant frequency bands that persist over time. These high-amplitude bands are primarily located in the low-frequency range between 16 and 64 Hz, corresponding to the frequency of the vortex rope's dominant oscillatory behavior. This suggests a strong coupling between pressure pulsations and the vortex rope dynamics, particularly in the low-frequency range, where the vortex rope is most active. The time-frequency analysis provides valuable insight into the frequency characteristics of pressure variations and their correlation with the underlying flow structures, helping to further elucidate the impact of cavitation and vortex dynamics on the overall system performance.

At the straight conical section of the draft tube, pressure pulsations are mainly induced by the periodic rotation of vortex ropes generated at the runner outlet. As these vortex ropes rotate, they transport low-pressure regions, which initiate localized cavitation. The blade passing frequency (f_{RSI}) of the runner couples with the dominant frequency of the vortex rope in this region, contributing to the observed low-frequency pressure pulsations. The recurring formation and collapse of cavitation bubbles also affect the pulsation signals within this frequency range. Due to flow instability, strong vortex disturbances and cavitation collapses exhibit nonlinear behaviour. The axial non-uniformity of the vortex ropes results in substantial variations in pressure pulsation intensity at different positions within the straight conical section, affecting the region's periodic characteristics. At monitoring points P6 and P7 in the bend of the draft pipe, the bright regions in the time-frequency diagrams are considerably diminished, and the overall brightness is reduced. This indicates that pressure pulsation intensity in the bent elbow is weaker compared to that in the straight conical section. As illustrated in the vortex rope analysis (Fig. 9), P6 is positioned above the bent elbow, distant from the main vortex core, and resides in a region characterized by minimal disturbances from secondary vortices or reverse flow. Consequently, it experiences less impact from intense pressure pulsations. The prominent areas in the frequency spectrum are almost non-existent; instead, only faint distributions are present, indicating limited influence from vortex ropes and cavitation. In contrast, P7 is positioned lower in the elbow section, closer to the vortex strip's rotational path. The disturbances generated by the high-speed rotation of the vortex strip directly impact the pipe wall, resulting in intermittent bright regions in the frequency spectrum, primarily within the 16 Hz to 32 Hz range. Comparison of the time-frequency spectra across the four monitoring points reveals that vortex ropes and cavitation are the primary sources of pressure pulsations in the draft pipe. However, their effects vary significantly based on the site of the monitoring points and the characteristics of vortex rope motion. The analysis also underscores the formation, interaction, and collapse of cavitation bubbles as critical contributors to the development of local bright regions. The axial non-uniformity of the vortex ropes, together with the distribution patterns of cavitation, jointly determine the spatial differences in pressure pulsation characteristics within the entire draft pipe.

The pressure pulsation characteristics observed in this study hold significant engineering implications for the smooth and stable performance of pump-turbines. Low-frequency pressure pulsations induced by the coupling of vortex ropes and cavitation may trigger structural vibrations, localized cavitation erosion, and even resonance risks. Identifying the source regions and frequency characteristics of these pulsations can contribute to optimizing the design of the draft tube, enhancing the unit's resistance to flow-induced disturbances, and providing a reference for defining the safe operating range of the governing system. Moreover, these findings collectively forge a theoretical foundation for the development of future monitoring and prediction models for pressure pulsations in pump-turbine systems.

4. CONCLUSION

This research elucidates the intricate coupling mechanism between the swirl ropes and cavitation in pump turbine drawworks, highlighting their evolution, development, and impact on flow stability and pressure pulsations. The results provide important theoretical

guidance for improving the operational stability and performance of pump turbines. Specifically,

1. The evolution of vortex ropes within the draft tube is governed by fluid rotation, pressure gradients, and structural features. Their dynamic behaviour holds considerable significance for the initiation and development of cavitation. Processes such as stretching, tearing, and the formation of low-pressure regions within the vortex ropes amplify cavitation effects. The rupture and collapse of cavitation bubbles destabilize the vortex structure while triggering the fragmentation and reformation of vortex ropes via pressure wave feedback, thereby intensifying flow instability. Meanwhile, observations indicate that the dynamic displacement and induced velocity fluctuations of vortex ropes are primary drivers of cavitation evolution. Alongside localized intensification of vortex strength, these factors shape the spatial distribution and cavitation's intensity characteristics in the draft tube.

2. High tangential momentum and shear layers drive the construction of alternating vortex structures adjacent to the runner outlet. These structures progressively dissipate downstream due to axial momentum transport, turbulence dissipation, and cavitation energy release. The flow field undergoes a transformation from an asymmetrical vortex-dominated state close to the outlet to a stable axisymmetric configuration further downstream. Simultaneously, the high-speed rotation and shear effects in the runner region markedly amplify cavitation fluctuations. The delayed cavitation response, which is induced by pressure wave feedback from the draft tube, underscores the dynamic coupling between the runner and the draft pipe.

3. The volume fluctuations of cavitation bubbles within the runner and draft tube regions exhibit periodicity and phase variations. In the draft tube, the peak-to-peak amplitude of cavitation volume amounts to approximately 1485 cm^3. This value is approximately 280 times larger than that in the runner (around 5.3 cm^3). The dominant oscillation frequency in the draft tube is slightly higher, indicating a close coupling with vortex rope rotation. This coupling, driven by the vortex rope's evolution, leads to the formation of a cavitation capture zone at the draft tube inlet. The phase lag between the cavitation volume in the runner and draft tube reflects the pressure wave propagation and feedback dynamics between the vortex structure and the pressure field. This coupling effect between the vortex and cavitation plays a vital role in comprehending cavitation-induced vibrations and flow stability.

4. The periodic rotation of the vortex rope and the collapse of cavitation bubbles represent the primary sources of pressure pulsations within the draft tube. In the straight conical section, low-frequency disturbances are predominantly driven by the coupling between vortex structures and cavitation dynamics, whereas in the elbow region, intermittent amplification of local pulsations arises from periodic interactions between the vortex rope and the pipe wall. These low-frequency pulsations exhibit distinct harmonic responses at integer multiples of the vortex rope's rotational frequency. The dominant frequencies are restricted to within 6.5 times the natural frequency (f_n) of the flow passage. Notable harmonic peaks are observed around 300 Hz, 600 Hz, and 900 Hz. Time-frequency analysis further reveals that pulsations within the 16–64 Hz range are the most pronounced in the straight conical section. These findings underscore the critical role of the spatiotemporal evolution of vortex rope structures and cavitation bubble dynamics in shaping the intensity distribution of pressure pulsations. They provide both theoretical foundation and practical engineering insights for assessing and optimizing the flow stability of the draft tube.

ACKNOWLEDGEMENTS

This research was funded by the National Natural Science Foundation of China (NSFC), under Grant No. 52066011.

CONFLICT OF INTEREST

The authors declare that they have no known competing financial interests or personal relationships that could have appeared to influence the work reported in this paper.

AUTHOR CONTRIBUTIONS

Lu Xin: Data curation, Writing-original draft Software, Writing-review; **Qifei Li:** Conceptualization, Software, Methodology; **Shiang Zhang:** Visualization, Investigation.

REFERENCES

Alekseenko, S. V., Kuibin, P. A., Shtork, S. I., Шторк, С., Skripkin, S., & Tsoy, M. (2016). Vortex reconnection in a swirling flow. *Jetp Letters, 103*(7), 455-459. https://doi.org/10.1134/s002136401607002x

Chen, A. (2017). *Study on vortex rope characteristics and improvement methods in pump-turbine draft tube.* Harbin Institute of Technology. https://doi.org/10.7666/d.D01335545

Chen, C., Li, D., Ji, Q., Wang, J., Xu,W. (2006). PIV Testing of Internal Flow Field within the draft tube of Francis Turbines. *Journal of Mechanical Engineering, 42*(12), 83-88. https://doi.org/10.1177/16878132241292399

Dragica, J. & Lipej, A. (2011). Numerical prediction of non-cavitating and cavitating vortex rope in a Francis turbine draft tube[J]. Strojniški vestnik-*Journal of Mechanical Engineering, 2011, 57*(6), 445-456. https://doi.org/10.5545/sv-jme.2010.068

Fanelli, M. (1989). The vortex rope within the draft tube of Francis turbines operating at partial load: a proposal for a mathematical model. *Journal of hydraulic research, 27*(6), 769-807. https://doi.org/10.1080/00221688909499108

Favey, H. T., & Cassidy, J. (1970). *Frequency and amplitude of pressure generated by swirling flow.* Proceedings of IAHR 5th Symposium. Stockholm: IAHR.

Goyal, R., Cervantes, M. J., & Gandhi, B. K. (2017a). Vortex rope formation in a high head model francis turbine. *Journal of Fluids Engineering-Transactions of The Asme, 139* (0411024). https://doi.org/10.1115/1.4035224

Goyal, R., Gandhi, B. K., & Cervantes, M. J. (2017b). Experimental study of mitigation of a spiral vortex breakdown at high Reynolds number under an adverse pressure gradient. *Physics of Fluids, 29*(10410410). https://doi.org/10.1063/1.4999123

Guo, Y., Kato, C., & Miyagawa, K. (2007). Large-eddy simulation of non-cavitating and cavitating flows within the draft tube of a Francis turbine. *Seisan Kenkyu, 59*(1), 83-88. https://www.jstage.jst.go.jp/article/seisankenkyu/59/1/59_1_83/_pdf

Han, F., Fan, C., Gui, Z., Zhang, W. (2006). Prediction of irregular pressure pulsations in unsteady flow in elbow-type draft tube. *Hydropower Generation, 32*(2), 49-51. https://doi.org/0559-9342(2006)05-0052-03

He, C., Wang, Z., & Qiu, H. (2002). experimental study on pressure pulsation inside the draft tube of turbines. *Journal of Mechanical Engineering, 38*(11), 62-65. https://doi.org/10.3969/j.issn.1006-7175.2002.02.038

Huang, J., Zhang, L., Wang, W., & Yao, J. (2011). Fine simulation of the three-dimensional unsteady flow separation vortex model in mixed-flow pump-turbines. *Proceedings of the CSEE, 31*(26), 83-89. https://doi.org/10.13334/j.0258-8013.pcsee.2011.26.006

Kavurmaci, B., Celebioglu, K., Aradag, S., & Taşcıoğlu, Y (2017). Model testing of Francis-type hydraulic turbines. *Measurement and Control, 50*(3), 70-73. https://doi.org/10.1177/0020294017702284

Li, J., Liu, S., Wu, Y., & Zhu, Y. (2010). Experimental and numerical simulation of the fly-away transition process in mixed-flow pump-turbines. *Large Electrical Machinery Technology, 2010*(6), 44-49. https://doi.org/1000-3983(2010)06-0044-06

Li, W., Li, Z., Han, W., Li, R., Zhang, Y. (2025). Mechanism of bubble generation in ferrofluid micro-pumps and key parameters influencing performance. *Powder Technology, 467*(15), 121562. https://doi.org/10.1016/j.powtec.2025.121562

Liao, W., Ji, J., Lu, P., & Luo, X. (2008). Effect of main shaft center hole aeration on internal flow in draft tube. *Journal of Hydraulic Engineering, 39*(8), 1005-1011. https://doi.org/0559-9350(2008)-1005-07

Litvinov, I., Shtork, S., Gorelikov, E., Mitryakov, A., & Hanjalić, K. (2018). Unsteady regimes and pressure pulsations in draft tube of a model hydro turbine in a range of off-design conditions. *Experimental Thermal and Fluid Science, 91*, 410-422. https://doi.org/10.1016/j.expthermflusci.2017.10.030

Liu, B., Yang, Q., Jiang, T., Zheng, Y., Zhang, Y. (2024) Analysis of Pressure Pulsation Characteristics and Vortex Belt Characteristics of Pump-Wheel Turbine Tail Water Chamber. *Rural Water Conservancy and Hydropower in China,* (07), 241-248. https://doi.org/10.12396/znsd.2319

Liu, J., Yang, J., Xiao, H., Yu, W., & Shen, C. (2006). Model experiment of pressure distribution at the inlet of draft tube during the transition process. *Journal of Wuhan University: Engineering Edition, 39*(1), 39-43. https://doi.org/1671-8844(2006)01-039-05

Liu, W., Qin, K., Xu, Y., & Wang, L. (2016). Model Test Study on Pressure Pulsation of Pump-turbine under turbine braking conditions. *Large Electric Machine Technology,* (3), 41-45. https://doi.org/1000-3983(2016)03-0041-05

Mulu, B. G., Jonsson, P., & Cervantes, M. J. (2012). Experimental investigation of a Kaplan draft tube - Part I: Best efficiency point. *Applied Energy, 93*(SI):695-706. https://doi.org/10.1016/j.apenergy.2012.01.004

Qi, J. (2017). Numerical simulation of francis turbine draft tube vortex and pressure pulsation. *Journal of Water Resources & Water Engineering, 28*(3):168-172. https://doi.org/10.1088/1755-1315/774/1/012089

Qian, Z., & Huang, S. (2006). Comparison of four turbulence models for cavitation flow simulation. *Advances in Water Science, 17*(2), 203-208. https://doi.org/1001-6791(2006)02-0203-06

Qu, L., & Wang, L. (1996). Study on pressure pulsation of mixed flow reversible pump-turbine across full operating conditions. *Power Engineering, 1996, 16*(6), 58-62. https://doi.org/10.1016/j.est.1996.101396

Skripkin, S. G., Tsoy, M. A., Kuibin, P. A., & Шторк, С (2017). Study of pressure shock caused by a vortex ring separated from a vortex rope in a draft tube model. *Journal of Fluids Engineering-Transactions of The Asme, 139*(0811038). https://doi.org/10.1115/1.4036264

Skripkin, S., Tsoy, M., Shtork, S., & Hanjalić, K (2016). Comparative analysis of twin vortex ropes in laboratory models of two hydro-turbine draft-tubes. *Journal of Hydraulic Research, 54*(4), 450-460. https://doi.org/10.1080/00221686.2016.1168325

Susan-Resiga, R., Dan Ciocan, G., Anton, I., Anton, I., & Avellan, F. (2006). Analysis of the swirling flow downstream a Francis turbine runner. *Journal of Fluids Engineering.* https://doi.org/10.1115/1.2137341

Tacob, T., & Liu S. (1998). Discussion on the pulsations of francis turbines and data processing. *Foreign Large Electric Machines, 1998*(3), 8.

Tamura, Y., Tani, K., & Okamoto, N. (2014). *Experimental and numerical investigation of unsteady behavior of cavitating vortices in draft tube of low specific speed Francis turbine.* IOP Conference Series: Earth and Environmental Science. IOP Publishing, *22*(3), 032011. https://doi.org/10.1088/1755-1315/22/3/032011

Tiwari, G., Kumar, J., Prasad,V., Patel, V. (2020). Derivation of cavitation characteristics of a 3MW prototype Francis turbine through numerical hydrodynamic analysis. *Materials Today Proceedings, 26*(2), 1439-1448. https://doi.org/10.1016/j.matpr.2020.02.297"

Wei, X. (1997). Experimental study on the control effect of stiffening plates on pressure pulsation in draft tube. *Large Electric Machine Technology,* (2), 73-78. https://doi.org/10.3969/j.issn.0559-9342.2007.02.022

Yang, J., Zhou, L., & Wang, Z. (2011). Numerical simulation of three-dimensional cavitation around a hydrofoil. *Journal of Fluids Engineering, 133*(8). https://doi.org/10.1115/1.4004385

Zhou, Y., Yu, X., Zhang, J., & Xu, H. (2024). The pressure pulsation characteristics during the load rejection transition process of a pump-turbine with split-flow blades. *Journal of Hydraulic Engineering, 55*(09), 1098-1109. https://doi.org/10.13243/j.cnki.slxb.20230781.

Zuo, Z., Liu, S., Liu, D., & Liu, D., Q, D. (2014). Numerical predictions and stability analysis of cavitating draft tube vortices at high head in a model Francis turbine. *Science China Technological Sciences, 57*(11), 2106-2114. https://doi.org/10.1007/s11431-014-5618-x